**Myoscaffolds demonstrate differential matrix components across muscular dystrophies**

Ashlee M. Long[1], Jason Kwon[1], Nina. L. Reiser[1], Lauren. A Vaught[1], Joseph G. O'Brien[1], Patrick G.T. Page[1], GaHyun Lee[1], Michele Hadhazy[1], Joseph C. Reynolds[2], Rachelle H. Crosbie[2], Elizabeth M. McNally[1*], and Alexis R. Demonbreun [1,3*]

[1]Center for Genetic Medicine, Northwestern University Feinberg School of Medicine, Chicago, IL 60611, USA
[2]Department of Integrative Biology and Physiology, UCLA, Los Angeles, CA; Department of Neurology David Geffen School of Medicine, UCLA, Los Angeles, CA
[3]Department of Pharmacology, Northwestern University Feinberg School of Medicine, Chicago, IL 60611, USA

*To whom correspondence should be addressed:
Alexis R. Demonbreun PhD
Center for Genetic Medicine
Northwestern University
303 E Superior SQ 5-512
Chicago, Il 60611 USA
T: 1 312 503 6249 F: 1 312 503 5603
alexis.demonbreun@northwestern.edu

Elizabeth M. McNally MD PhD
Center for Genetic Medicine
Northwestern University
303 E Superior SQ 5-516
Chicago, Il 60611 USA
T: 1 312 503 5600 F: 1 312 503 5603
elizabeth.mcnally@northwestern.edu

**Conflicts:** Northwestern University filed provisional patents #62/783,619 and #63/309,925 on behalf of the authors (ARD and EMM). The other authors have declared that no conflict of interest exists.

**Abbreviations:** Extracellular matrix (ECM), decellularized extracellular matrix (dECM), Duchenne Muscular Dystrophy (DMD), Limb Girdle Muscular Dystrophy (LGMD), sodium dodecyl sulfate (SDS)

**Keywords:** Extracellular matrix, Duchenne muscular dystrophy, Limb Girdle muscular dystrophy, muscle

**ABSTRACT**

Pathological remodeling of the extracellular matrix (ECM) underlies many fibrotic disorders, including muscular dystrophy. In fibrotic disorders, large matricellular proteins like proteoglycans and glycoproteins, and smaller secreted factors are progressively deposited into the matrix. Tissue decellularization uses detergent treatment to remove the cellular component, leaving behind intact the matrix components. Decellularized ECMs (or dECMs) have most commonly been studied in intact organs, but more recently, this method has been adapted to tissue sections on slides. We generated dECM from genetically different mouse models of muscular dystrophies including dystrophin-deficient, γ-sarcoglycan-deficient, and dysferlin-deficient mice, as well as analyzing distinct background mouse strains known to alter the ECM. Formalin fixed samples were assessed for complete decellularization, preservation of ECM architecture, and protein retention using histological staining and immunofluorescence microscopy. Excess collagen deposition correlated with fibrosis severity across the different dystrophic models. Each muscular dystrophy subtype demonstrated excess decorin deposition in the matrix. Dystrophin- and γ-sarcoglycan-deficient muscles displayed excess thrombospondin 4, while dysferlin-deficient muscle had excess decorin but not excess thrombospondin 4. Annexins A2 and A6 were increased across all dystrophic dECMs, but annexin deposition was greatest in dysferlin-deficient muscular dystrophy. In this model, annexin A2 was diffusely increased but annexin A6 was found in discrete regions of marked excess protein within the matrix. These studies highlight the differential nature of the core matrisome and its associated proteins in different forms of muscular dystrophy, where these proteins are positioned to influence the surrounding myofibers and inflammatory infiltrate.

## INTRODUCTION

Muscular dystrophies are a group of heterogenous disorders characterized by progressive muscle degeneration and loss of muscle strength. Mutations that disrupt formation of the dystrophin glycoprotein complex (DGC), a group of proteins essential for sarcolemma stability, result in multiple forms of muscular dystrophy. Duchenne muscular dystrophy (DMD) is caused by mutations in the dystrophin gene, a central scaffold within the DGC, that links the cytoskeleton to the extracellular matrix (Campbell and Kahl, 1989; Monaco et al., 1986; Rando, 2001). The sarcoglycan complex, is a sub-complex of the DGC. Recessive loss-of-function mutations in sarcoglycans α-, β-, δ-, γ- result in distinct subtypes of Limb Girdle muscular dystrophy (LGMD), (Lim et al., 1995; Nigro et al., 1996; Noguchi et al., 1995). Destabilization of the muscle membrane that occurs in these muscular dystrophies, leads to chronic muscle damage, persistent inflammation, and progressive fibrofatty replacement of muscle tissue, ultimately impairing muscle function. Beyond membrane stabilization, maintenance of the muscle membrane is required for cellular homeostasis and proper tissue function. Excessive muscle contraction and trauma can also induce membrane rupture, requiring a quick and efficient means of repair to prevent cellular necrosis. Dysferlin is a calcium-dependent, phospholipid binding protein that facilities muscle membrane repair (Bansal et al., 2003; Bashir et al., 1998; Davis et al., 2002; Defour et al., 2014; Lek et al., 2012; McDade et al., 2014). Loss-of-function mutations in *DYSF*, the gene encoding dysferlin, lead to Limb Girdle muscular dystrophy 2B (LGMD2B) and Myoshi Myopathy (MM) (Bashir et al., 1998; Liu et al., 1998). Continual membrane leak in dysferlinopathy leads remarkably high serum creatine kinase levels, proximal muscle weakness, and inflammatory infiltrate such can lead to misdiagnosed as polymyositis (Contreras-Cubas et al., 2022).

Mouse models recapitulate many of the pathological features seen in the human muscular dystrophies (Ceco et al., 2014; Coley et al., 2016; Hack et al., 1998; Hammers et al., 2020; Ho et al., 2004; Lostal et al., 2010; Sicinski et al., 1989; van Putten et al., 2020). The most commonly used mouse model, the *mdx* mouse, harbors a single point mutation in exon 23, resulting in loss of full-length dystrophin (Sicinski et al., 1989). Despite loss of dystrophin, *mdx* mice on the C57BL/10 background exhibit relatively mild muscle disease compared to humans with DMD. In the *mdx* mouse, advanced muscle fibrosis and cardiomyopathy do not occur until late in life, and still remain milder than their human counterparts. Genetic background can shift the pathological and functional manifestations of muscular dystrophy (Gordish-Dressman et al., 2018; Heydemann et al., 2005). Specifically, the DBA/2J strain was shown to intensify membrane fragility and fibrosis in *Sgcg null* mice, which lack the dystrophin-associated protein γ-sarcoglycan (Heydemann et al., 2005). Similarly, the *mdx* mouse displays greater muscle damage, increased inflammation and increased intramuscular fibrosis in the DBA/2J strain compared to the C57BL/10 strain at an early age (Coley et al., 2016).

The increase in disease severity conferred by the DBA2/J background has been attributed to a number of genetic modifiers including latent TGF-β binding protein 4 (LTBP4), osteopontin (OPN/SPP1), and annexin A6 (ANXA6) (Heydemann et al., 2009; Swaggart et al., 2014). Several of these modifiers are known extracellular matrix proteins, suggesting a role for the matrix in muscle disease progression. LTBP4 is an extracellular glycoprotein that binds and sequesters TGF-β, modulating downstream TGF-β activity, controlling fibrosis formation (Ceco et al., 2014; Flanigan et al., 2013; Heydemann et al., 2009). OPN is a matrix glycoprotein that is upregulated in muscle disease, promoting pro-inflammatory macrophage polarization and enhancing TGF-β activity contributing to fibrosis formation (Capote et al., 2016; Kramerova et al., 2019; Pegoraro et al., 2011). ANXA6 is a known membrane repair protein that acts as a molecular band-aid, aiding in membrane resealing, improving repair capacity upon membrane injury (Boye et al., 2017; Croissant et al., 2020; Demonbreun et al., 2016; Swaggart et al.,

2014). The role of ANXA6 within the extracellular matrix of muscle is less defined but, as a protein class, annexins have been implicated in cellular migration and differentiation (Belvedere et al., 2014; Bizzarro et al., 2012; Garcia-Melero et al., 2016; Grewal et al., 2017).

The extracellular matrix (ECM) in muscle influences myofibers and muscle regeneration. In the muscular dystrophies, the matrix becomes highly abnormal with increased fibrofatty deposition (Dowling et al., 2021). In healthy muscle, the ECM includes collagens, glycoproteins, and proteoglycans, and serves as a scaffold for signaling proteins, regulators and secreted factors, like TGF-β. After muscle injury, ECM content shifts during the repair and recovery process, similar to scar retraction in skin. In muscular dystrophy however, there is ongoing and repetitive injury concomitant with attempted repair. Muscular dystrophy is characterized as having abnormal excess matrix formation which can impair myoblast differentiation and promote fibroblast activity (Loreti and Sacco, 2022; Thomas et al., 2015). Additionally, genetic mutations in core ECM proteins like collagen and laminin can result in COL6-related disorders Bethlem and Ullrich muscular dystrophy and LAMA2-associated congenital muscular dystrophies respectively, illustrating the critical nature of an intact matrix (Bonnemann et al., 2014; Mendell et al., 2006). Given the role of excess matrix in contributing to muscular dystrophy pathology, we employed and optimized a recently described method of generating myoscaffolds and compared ECM in different muscular dystrophy subtypes (Stearns-Reider et al., 2022).

We explored ECM composition across multiple mouse models of muscular dystrophy at a timepoint of established disease and identified patterns of ECM proteins, including both core matrisome and matrisome associated proteins in different muscular dystrophies. Decellularized ECM (dECM) studies rely on scaffolds obtained from tissues where the cellular component has been removed allowing examination of the acellular ECM. This process exposes certain proteins that may normally be masked by cellular content. We showed this detergent-based procedure reproducibly generated high quality and reproducible dECMs from healthy and dystrophic tissue. We found that ECM from *mdx* in the DBA/2J (D2) background had the most significant increase in matrisomal protein expression of decorin, periostin, thrombospondin 4 and matrix metalloproteinase 9, compared to *mdx*, dysferlin-null and wildtype healthy controls. This pattern was similar to dECMs from *Sgcg* mice in the DBA/2J background, suggesting an essential role for genetic background. Interestingly, dysferlin-null mice exhibited the highest expression of matrix-associated annexin A2 and annexin A6. Our work highlights the disease specific differences in ECM composition that are positioned to modulate disease progression.

## RESULTS

*Generation of acellular myoscaffolds using chemical decellularization.* For more than a decade, decellularized scaffolds have been generated from heart and muscle and studied for their ability to support cellular regeneration (reviewed in (Tan et al., 2022)). Recently Stearns-Reider et al published an "on-slide" decellularization method using 30µm tissue sections exposed to 1% SDS for 40 mins to generate dECM myoscaffolds (Stearns-Reider et al., 2022). We replicated the method and further optimized the generation of dECM scaffolds to ensure reproducible removal of intracellular components and DNA, while retaining ECM architecture and function. Chemical decellularization was attempted using a sodium dodecyl sulfate (SDS) solution. WT and *mdx* muscles were incubated in a 1% SDS solution for 10-30 minutes. Removal of the cellular components after decellularization was assessed through hematoxylin and eosin (H&E) staining, with complete decellularization observed at 10 minutes (**Figure 1A**). Decellularization was attempted with 0.1% SDS for 0-60 minutes to ascertain if a reduced concentration of SDS would be more appropriate (**Figure 1B**). At the reduced concentration, remaining cellular components were observed at time points 20-40 minutes, but complete decellularization observed after a 60-minute incubation with 0.1% SDS (**Figure 1B**). These data support that decellularization with complete removal of the cellular components is achievable using SDS for both WT and *mdx* tissues after a 10-minute incubation period for 1% SDS concentration. All other decellularization experiments in this study utilized a 1% SDS concentration for a 10-minute incubation period on sections generated from quadriceps muscles.

*Acellular myoscaffolds retain key ECM proteins and architectural integrity.* To further assess the effectiveness of the decellularization method, we performed quality checks on the decellularized extracellular matrix (dECM). dECMs were generated from well-characterized muscular dystrophy models lacking dystrophin, sarcoglycan or dysferlin proteins that vary in disease severity: WT, *mdx*, *mdxD2*, *BLAJ*, *Sgcg*, *SgcgD2*, and *mdxhLTBP4* (Ceco et al., 2014; Demonbreun et al., 2019b; Hack et al., 1998) (**Table 1**). *mdx*, and *mdxD2* represent both mild and severe forms of muscular dystrophy, while *Sgcg* and *SgcgD2* represent an LGMD model and also reflect differences in genetic background. *BLAJ* mice represent a distinct LGMD, which is due to loss of dysferlin, a membrane repair protein. Matrix quality was assessed following decellularization to determine retention of key proteins and architectural integrity (Crapo et al., 2011; Gilpin and Yang, 2017). Complete removal of the cellular components in the dECMs across all strains was confirmed by Hematoxylin and Eosin (H&E) staining (**Figure 2A**). Sirius Red staining evaluated collagen deposition and integrity in the generated acellular myoscaffolds (**Figure 2B**). Intact collagen structure was visualized within the dECMs with increased collagen deposition observed in more severe muscular dystrophy models as expected (*mdxD2* > *mdx* > WT). Retention of ECM glycosaminoglycans (GAGs) post decellularization was confirmed with Alcian Blue staining (**Figure 2C**).

The architectural integrity of the acellular myoscaffolds was further interrogated through immunofluorescence microscopy (IFM) of laminin and collagen pre- and post-decellularization. Antibodies against laminin-2 and collagen type 1 demonstrated intact laminin and collagen within the dECM scaffolds across all strains (**Figure 3A-B**). Interestingly, both ECM proteins were more easily visualized in the acellular scaffolds. This is consistent with previous literature demonstrating increased collagen quantification after decellularization, hypothesized to be due to epitope exposure after cellular removal (Baptista et al., 2011; Hussein et al., 2016; Stearns-Reider et al., 2022). Elimination of nucleic acids was confirmed through Hoechst staining (**Figure 3C**). Additionally, DNA remnants were evaluated by isolating DNA from decellularized and non-decellularized tissue sections. Isolation and quantification of DNA demonstrated a reduction of DNA post 1% SDS decellularization to an acceptable level of less than 50ng dsDNA per mg ECM (**Supplemental Figure 1**) (Crapo et al., 2011). These data demonstrate

that a 10-minute incubation with a 1% SDS solution results in intact decellularized matrices, that are devoid of cellular components and nucleic acids while retaining core components of ECM maintaining architectural integrity.

*Core Matrisome Proteins across different muscular dystrophy subtypes*. ECM proteins are referred to the matrisome, which can be separated into "core" and "associated" matrisome proteins (Naba et al., 2016; Shao et al., 2019). Core matrisome proteins include nearly 275 proteins which fall into three categories: glycoproteins (194), collagens (44), and proteoglycans (36) (**Figure 4A**) (Naba et al., 2016; Shao et al., 2019). We selected specific core matrisome proteins to examine in acellular dECM myoscaffolds from distinct muscular dystrophy subtypes. Periostin (POSTN), thrombospondin-4 (THBS4), and decorin (DCN) were studies since each of these proteins has been previously evaluated in muscular dystrophy models (Caceres et al., 2000; Chen et al., 2000; Fadic et al., 2006; Lorts et al., 2012; Vanhoutte et al., 2016; Zanotti et al., 2005) (**Figure 4B**). After decellularization, acellular myoscaffolds from each mouse strain, were probed with antibodies to DCN, POSTN, and THBS4; representative images are shown in **Figure 4C**. All three proteins exhibited increased signal in the more severely fibrotic models of muscular dystrophy (**Figure 4C and 4D**). Increased expression of DCN, POSTN, and THB4 was observed in the myoscaffolds of *mdxD2* compared to *mdx* and increased in *mdx* compared to WT (**Figure 4D**). The *BLAJ* dECM exhibited a distinct pattern of expression, with DCN, POSTN, and THBS4 signal similar to or decreased when compared to *mdx* dECM. THBS4 was observed in a vesicle-like pattern in the ECM (**Figure 4E**; thin white arrow) compared to POSTN, which demonstrated a more diffuse expression pattern (**Figure 4E**; thick white arrows). Quantitative analysis of the fluorescence patterns of DCN, POSTN, and THBS4 protein expression on the acellular myoscaffolds of WT, *mdx*, *mdxD2*, and *BLAJ* is shown in **Figure 4F-H**. DCN, POSTN, and THBS4 intensity was significantly increased in *mdxD2* acellular dECM myoscaffolds compared to *mdx* and WT matrices. Fluorescence intensity was also increased in *mdx* compared to WT for DCN and POSTN. A consistent pattern of WT < *mdx* < *mdxD2* was observed (**Figure 4F-H**). The acellular myoscaffolds generated from the BLAJ mouse model demonstrated significantly less matrix protein compared to *mdxD2* for all three core matrisome proteins analyzed, with protein levels trending similarly with the *mdx* scaffolds for POSTN and DCN (**Figure 4F and G**). Interestingly, THBS4 levels in BLAJ dECMs were most similar to WT THBS4 levels (**Figure 4H**). Immunoblotting of soluble and insoluble muscle fractions isolated from WT, *mdx*, *mdxD2*, and BLAJ mice for DCN, POSTN, THBS4 mirror the quantitation of IFM dECM (**Supplemental Figure 2**). These data show a unique distribution of core matrisomal proteins across different forms of muscular dystrophy.

*Matrisome-Associated Proteins, MMP9, TIMP-1, and TGF-β1, were retained in acellular myoscaffolds.* The matrisome associated protein category consists of over 800 proteins separated into three sub-categories: Secreted Factors (367), ECM-Affiliated (165), and Regulators (304) (**Figure 5A**) (Naba et al., 2016; Shao et al., 2019). We evaluated muscular dystrophy relevant proteins from each category including annexin A2 (ANXA2), annexin A6 (ANXA6), matrix metalloproteinase-9 (MMP9), TIMP metallopeptidase inhibitor 1 (TIMP-1), and transforming growth factor beta 1 (TGF-β1) (**Figure 5B**). After decellularization, the acellular myoscaffolds were probed with antibodies to MMP9, TIMP-1, or TGF-β1 for each model. Representative images demonstrated increased protein expression in dECMs from the most severely fibrotic models of muscular dystrophy (**Figure 5C**). To determine any differences in protein deposition, WT, *mdx*, *mdxD2*, and *BLAJ* dECMs were probed for MMP9, TIMP-1, or TGF-β1 and merged with the anti-laminin signal (**Figure 5D**). TIMP-1 was visualized as ubiquitously expressed throughout the matrix of all strains analyzed, while MMP9 and TGF-β1 were observed in distinct localization patterns. In *mdxD2* dECM, 100x Z-stack representative

images demonstrated a vesicle-like pattern of MMP9 protein distinct from the diffuse TIMP-1 expression pattern (**Figure 5E**). Increased expression of MMP9 and TGF-β1 was seen in dystrophic dECMs, with *mdxD2* exhibiting significantly greater matrix protein compared to *mdx*, and *mdx* expression levels greater than WT (**Figure 5F-5H**). dECM myoscaffolds from dysferlin-deficient *BLAJ* muscle tissues exhibited MMP9 and TGF-β1 protein levels similar to or slightly increased compared to *mdx*, respectively. TIMP-1 expression was increased over WT in a similar fashion across *mdx*, *mdxD2*, and *BLAJ* (**Figure 5F-5H**). These data show that the acellular dECM myoscaffolds retained key core and matrisome-associated proteins and these patterns differed significantly across different muscular dystrophy subtypes.

*Annexins A2 and A6 were significantly increased in BLAJ dECM compared to other muscular dystrophy myoscaffolds.* The annexin protein family members, including annexin A2 and A6, belong to the matrisome-affiliated category in the subcategory of ECM-affiliated proteins ((Naba et al., 2016; Naba et al., 2012; Shao et al., 2019); matrisome.org). The acellular dECM myoscaffolds were probed with antibodies to ANXA2 and ANXA6. Immunofluorescence imaging demonstrated increased ANXA2 and ANXA6 in the matrix of more severely fibrotic models of muscular dystrophy including *mdxD2* and *SgcgD2* (**Figure 6A**). The ANXA2 and ANXA6 pattern was evaluated in reference to the laminin pattern in WT*, mdx*, *mdxD2*, and *BLAJ* dECMs (**Figure 6B-6G**). Interestingly, these two annexins display different expression profiles with ANXA2 exhibiting low-level, diffuse expression within the matrix, while ANXA6 was more abundant in vesicle-like structures. Z-stack images showed the increased accumulation of ANXA6 vesicles in the dECM of BLAJ scaffolds (**Figure 6B and 6D**; thin white arrow). However, in more saturated areas, ANXA6 appeared as a solid rim over the laminin, surrounding what remained of the acellular myofibers (**Figure 6D**; thick white arrow). Additionally, strong ANXA6 signal was distributed throughout the majority of the *BLAJ* dECM myoscaffold, while ANXA2 was expressed in focal regions (**Figure 6E**). Quantitative fluorescent intensity analysis indicated that ANXA2 and ANXA6 in *mdxD2* acellular dECM myoscaffolds were increased compared to WT, as expected (**Figure 6B-6G**). Surprisingly ANXA2 and ANXA6 were significantly increased in *BLAJ* dECMs compared to *mdxD2* (**Figure 6F-6G**), unlike the other matrisomal proteins analyzed (**Figures 4 and 5**). These data demonstrate a significant difference in the muscle extracellular matrix composition from mice lacking dysferlin compared to those that lack dystrophin.

## DISCUSSION

*Generation of dECM myoscaffolds from muscular dystrophy models.* These acellular myoscaffolds are useful as a tool for studying differential matrisome profiles. The process of tissue decellularization has been widely used in regenerative medicine due to the inherent biological signaling properties remaining in the scaffolds that support recellularization. Historically the focus has been on whole tissue and minced tissue decellularization utilizing sodium dodecyl sulfate (SDS) or Triton x-100 as decellularization agents (Gilpin and Yang, 2017; Mendibil et al., 2020). Decellularized matrices are often ground and solubilized to create bioink harboring these potent molecules for use in 3D printing. Decellularized extracellular matrices have also been utilized as a 3D *in vitro* culture system to have more physiologically relevant conditions to better study cellular behavior (Hakkinen et al., 2011; Harris et al., 2018; Hoshiba, 2019). By using decellularized tissue sections to evaluate, we were able to highlight elements of the distinct ECM protein profiles in different mouse models of muscular dystrophies. In healthy skeletal muscle, the ECM provides a supportive microenvironment regulating cellular adhesion, migration, proliferation, and differentiation and is essential for maintaining muscle function (Meyer and Lieber, 2011). In muscle diseases like the muscular dystrophies, excessive matrix accumulates in the muscle resulting in tissue dysregulation (Dowling et al., 2021). The spatial patterning and matrix stiffness is altered in muscular dystrophy, which is positioned to alter cellular behavior and differentiation (Chen and Li, 2009). The method and results described in this current work can ultimately be adapted to evaluate how the spatial differences across diseased and healthy muscle matrices can influence surrounding cells.

We found that the *mdxD2* model with more severe fibrosis had significantly increased levels of core matrisomal proteins THBS4, POSTN, and DCN within the dECM scaffolds. THBS4 is a core matrisomal protein that regulates muscle attachment at the myotendinus junction and promotes sarcolemmal stability. THBS4 is upregulated in muscle biopsies from humans with Duchenne, Becker and Limb Girdle muscle dystrophies and their corresponding mouse models (Brody et al., 2018; Chen et al., 2000; Subramanian and Schilling, 2014; Vanhoutte et al., 2016). Overexpression of THBS4 in muscle using transgenesis is sufficient to protect against muscular dystrophy disease progression by stabilizing the sarcolemma through enhanced trafficking of the dystrophin-glycoprotein and integrin attachment complexes (Brody et al., 2018; Vanhoutte et al., 2016). Moreover, secretion of THBS4 was shown to be an essential component to elicit these protective effects. Secretion-deficient THBS4 was associated with an increased in intracellular vesicles visualized by electron microscopy. The THBS4 expression we now observed in *mdxD2* myoscaffolds was seen in puncta throughout the matrix. These puncta likely derive from the normal secretion of THBS4 vesicles, and support a role for THBS4 in transporting matrix-bound molecules.

*TGF-β regulation in the extra-cellular matrix of dystrophic muscle.* TGF-β is a key regulator of fibrosis formation with increased TGF-β levels correlating with more severe disease pathology (Dadgar et al., 2014). The *mdxD2* mouse harbors a polymorphism within the *LTBP4* gene, encoding LTBP4, a protein responsible for regulating TGF-β bioavailability (Heydemann et al., 2009). This *LTBP4* polymorphism has been associated with increased TGF-β regulated SMAD signaling and more severe muscle fibrosis (Ceco et al., 2014; Hammers et al., 2020; Heydemann et al., 2009). Consistent with greater ECM fibrosis visualized by Sirius red staining, we observed increased TGF-β1 deposition in myoscaffolds generated from *mdxD2* mice compared to the dECMs generated from *mdx* and WT mice. TGF-β release and activation is regulated by multiple independent co-regulators which fine tune local and/or tissue-specific TGF-β responses. Decorin (DCN) is a small proteoglycan that binds and neutralizes TGF-β preventing fibrosis formation and improving muscle regeneration (Li et al., 2007). DCN is

increased in the matrix of DMD muscle biopsies, likely due to the increased synthesis of DCN by DMD fibroblasts (Caceres et al., 2000; Fadic et al., 2006; Zanotti et al., 2005). The increased DCN in dECM myoscaffolds from the more fibrotic *mdxD2* skeletal muscle is highly consistent with the human and mouse data. Iqbal et al. demonstrated the usefulness of utilizing ECM proteins in the development of a lesion-homing, recombinant CAR-decorin fusion protein that induced lesion-specific TGF-β inhibition (Iqbal et al., 2021). This targeted delivery method resulted in decreased fibrosis with improved skeletal muscle function in *mdxD2* mice.

Periostin (POSTN) is also implicated in regulating fibrosis severity. Not only is POSTN regulated by TGF-β, but POSTN is also required for normal TGF-β signaling (Snider et al., 2008). POSTN is normally expressed at low levels in healthy tissues, but its expression is increased after acute injury and in muscular dystrophies. Unlike THBS4, overexpression of POSTN exacerbated muscle disease progression and promoted fibrosis formation in *Sgcd*-null mice, a model of LGMD2F (Lorts et al., 2012). Conversely, reduction in THBS4 mitigated disease progression. In dECMs POSTN expression was increased in the more severe *mdxD2* dECM compared to the mild *mdx* and WT dECMs. We hypothesize that the increased TGF-β levels in this model upregulates *Postn* expression while *Dcn* is upregulated as a compensatory protective mechanism.

These unique ECM protein profiles offer insights into differential cellular behavior. POSTN and DCN are known inhibitors of myoblast migration and differentiation. Stearns-Reider et al. demonstrated that skeletal muscle progenitor cells seeded into heavily fibrotic areas of *mdx* dECM scaffolds had reduced migratory capacity, a rounded morphology, and reduced differentiation potential compared to mildly-fibrotic areas of *mdx* and WT matrices (Stearns-Reider et al., 2022).

*Differential matrix-associated annexins A6 and A2 accumulation in dysferlin-null and dystrophin-null muscle matrices.* We demonstrated in acellular myoscaffolds differential annexin A6 and A2 expression and localization in the dystrophic models studied. Annexin A6 functions to facilitate the repair complex formation upon muscle membrane injury, forming an annexin-rich cap that sits above the dysferlin-containing shoulder region at the membrane lesion (Demonbreun et al., 2016; Roostalu and Strahle, 2012). Similar to annexin A6, annexin A2 also localizes to the repair cap at the site of membrane injury and is present in extruding vesicles (Demonbreun et al., 2019a; Roostalu and Strahle, 2012). Although both annexin A6 and A2 are present in the repair cap and emanating vesicles, *in vitro* studies illustrate distinct roles for annexin A6 and annexin A2 in mediating membrane repair. Specifically, annexin A2 facilities membrane folding and formation of vesicles from a central site of membrane imperfection compared to annexin A6 which prefers acting on the membrane free edge (Boye et al., 2018). *In vitro* studies using recombinant annexin A6 and artificial membrane demonstrated that annexin A6 acts to pull the membrane wound edges together enhancing closure (Boye et al., 2017). Studies on live isolated myofibers showed that annexin A6 can facilitate membrane resealing from both intracellular and extracellular compartments suggesting a potential role for extracellular annexins in resealing (Demonbreun et al., 2022; Demonbreun et al., 2019a). The distinct localization patterns between annexin A6 (vesicular) and A2 (diffuse) in the dECM scaffolds) suggests the likelihood of differential origins of these matrix proteins. Immunofluorescence imaging of non-decellularized 12-month-old BLAJ muscles showed annexin A2 accumulation in the interstitial space which correlates with fibroblast markers PDGFRa and perilipin-1 (Hogarth et al., 2019). We hypothesize that fibroblasts may be the additional source of annexin A2, as the diffuse pattern resembles the pattern of fibroblast secreted POSTN and DCN.

Dysferlin's role in mediating sarcolemmal repair is distinct from dystrophin's role of stabilizing the sarcolemma. Mice lacking both dysferlin and dystrophin displayed a more intense phenotype, reflect by increased pathology, serum creatine kinase, Evan's blue dye

uptake and susceptibility to eccentric contraction induced injury compared to the mice lacking dysferlin or dystrophin alone (Han et al., 2011). The distinct annexin protein patterns observed in *mdx* and *BLAJ* dECMs highlight the differences in the pathogenesis of these two diseases. We hypothesize that in the repair of incompetent dysferlin-deficient *BLAJ* myofibers, recruitment of annexin A6 to the membrane lesion is enhanced to compensate for the lack of dysferlin. Through immunofluorescence microscopy and correlative light and electron microscopy (CLEM), annexin A6- positive vesicles have been visualized emerging from the membrane lesion seconds to minutes post rupture (Croissant et al., 2020; Demonbreun et al., 2019a). With DIC imaging, Roman and colleagues visualized a repair like structure with emanating vesicles that persists for at least 24 hours post muscle membrane injury, during a period referred to as myofiber rebuilding (Roman et al., 2021). It is plausible that the vesicles identified in the dECM scaffolds are those released from the injured myofiber repair caps. Together, the study of dECMs from multiple muscular dystrophy models highlight differences which afford insight to the distinct pathology of these muscle degenerative diseases.

## MATERIALS AND METHODS

**Animals.** All animals were bred and housed in a pathogen free facility. Wild-type (WT) mice were from the C57BL/6 strain. C57BL/10ScSn-*Dmdmdx*/J (*mdx*), D2.B10-*Dmdmdx*/J (*mdxD2*), and B6.A-*Dysfprmd/*GeneJ (*BLAJ*) mice were originally purchased from The Jackson Laboratory (strains #:001801, #:013141, and #:012767 respectively). Sarcoglycan γ-null (*Sgcg*) mice were previously generated on the C57BL/6 background, Sgcg 521ΔT (*SgcgD2*) were previously generated on the DBA2/J background and *mdxhLTBP4* mice were previously generated on the C57BL/6 background (Ceco et al., 2014; Demonbreun et al., 2019b; Hack et al., 1998). Seven- to eight-month-old male and female mice were used for all experiments. Mice were bred and housed in a specific pathogen free facility on a 12-hour light/dark cycle and fed *ad libitum*.

**Study Approval.** All procedures using mice followed *Guide for the Care and Use of Laboratory Animals* and were approved by Northwestern University's Institutional Animal Care and Use Committee.

**Decellularization.** Quadriceps muscle was harvested and flash frozen in liquid nitrogen. Sections were cryosectioned at 25um (Leica CM1950) and mounted on charged Superfrost Plus Microscope Slides (cat# 1255015; Fisher Scientific). Slides were stored at -80°C. Decellularization was performed as in Stearns-Reider et al.,2022 with the following modifications (Stearns-Reider et al., 2022). Slides were allowed to thaw to room temperature for 1 hr prior to decellularization. Slides were then placed in a 15mL UltraPure Sodium Dodecyl Sulfate (SDS) solution (cat# 15553035; Invitrogen) diluted with PBS to 0.1, 0.5, or 1% concentration for 10 minutes under constant agitation (40 rpm). Slides were then placed in 100mm x 100mm square petri dishes 3 slides per dish (Fisher cat#FB0875711A) containing 13mL of PBS (with calcium & magnesium [Cat# 21030CV; Corning]), for 10 minutes, then placed in a fresh 13mL of PBS for 45 minutes, followed by 13mL UltraPure Distilled $H_2O$ (cat# 10977015; Invitrogen) for 30 minutes, and a final 13mL PBS wash for 45 minutes. All wash steps were done under constant agitation (40 rpm). Decellularized slides were either fixed for histology/immunostaining or stored in PBS.

**DNA Extraction.** DNA was extracted from quadriceps muscle tissues using the DNeasy Blood & Tissue Kit (cat# 69504; Qiagen) and DNA concentration measured on a NanoDrop 2000 Spectrophotometer (Thermo Scientific). DNA electrophoresis was visualized using a BioSpectrum Imaging system Chemi 410 (UVP).

**Histology.** Quadriceps muscle was harvested and fixed in 10% formalin. Hematoxylin and eosin (cat# 12013B and 1070C; Newcomer Supply), Sirius Red (cat# 24901250; Polysciences, Inc), or Alcian Blue (cat#A3157; Sigma) staining was performed per manufacturer's protocol. All images were acquired on the Keyence BZ-X810 microscope with a 40x objective and same exposure settings across all genotypes.

**Protein isolation.** *Tibialis anterior* muscles were harvested and flash-frozen in liquid nitrogen. Tissues were ground with a mortar and pestle and lysed in Whole Tissue Lysis buffer (50mM HEPES pH 7.5, 150mM NaCl, 2mM EDTA, 10mM NaF, 10mM Na-pyrophosphate, 10% glycerol, 1% Triton X-100, 1mM phenyl-methylsulfonyl fluoride, 1x cOmplete Mini protease inhibitor cocktail [cat # 11836170001; Roche], 1x PhosSTOP [cat# 04906837001; Roche]) and homogenized using a TissueLyser II (Qiagen) at a frequency of 30.0 1/s and time of 2.00 min/sec for 6 rounds. Protein lysates were then centrifuged at 20,000xg for 20 minutes to separate the soluble and insoluble fractions. The soluble supernatant layer was placed in a

separate tube and the insoluble pellet layer was resuspended with an 8M Urea buffer (8M Urea [cat#U4883; MilliporeSigma], 2mM EDTA, 10mM DTT, 1x cOmplete Mini protease inhibitor cocktail [cat # 11836170001; Roche]). The protein concentration was measured with the Quick Start Bradford 1x Dye Reagent (cat# 5000205; Bio-Rad Laboratories).

**Immunoblotting.** 20-25ug of protein lysate with 4x Laemmli buffer (cat# 1610747; Bio-Rad Laboratories was separated on 4-15% Mini-PROTEAN TGX Precast Protein Gels (cat# 4561086; Bio-Rad Laboratories) and transferred to Immun-Blot PVDF Membranes for Protein Blotting (cat# 1620177; Bio-Rad Laboratories). Membranes were reversibly stained for total protein with Ponceau S Staining Solution (cat# A40000278; Thermo Scientific) to ensure transfer and equal loading prior to antibody incubation. Blocking and antibody incubations were done using StartingBlock T20 (TBS) Blocking Buffer (cat# 37543; Thermo Scientific). Primary antibodies were used at 1:1000 except for anti-thrombospondin-4 and anti-TIMP-1 which were diluted at 1:100. Secondary antibodies conjugated with horseradish peroxidase were used at 1:2,500 (cat# 111035003; Jackson ImmunoResearch Laboratories). Clarity Western ECL Substrate (cat# 1705061; BioRad Laboratories) was applies to membranes and visualized using an iBright 1500 Imaging System (Invitrogen). Pierce Reversible Protein Stain Kit for PVDF Membranes (including MemCode; cat# 24585; Thermo Fisher Scientific) was used to ensure equal loading.

**Immunostaining and immunofluorescence imaging.** Decellularized quadriceps cryosections (dECMs) were fixed in 4% paraformaldehyde, rinsed, and blocked with a 1% BSA/10% FBS blocking buffer for 1 hour. The dECMs were incubated with the primary antibodies overnight at 4°C at 1:100. The dECMs were then incubated with the secondary antibodies at 1:2,500 for 1 hr. The dECMs were mounted with ProLong Gold Antifade Reagent (cat# P36934; Invitrogen) and images acquired on a Keyence BZ-X810 microscope with 20x, 40x, 60x and 100x objectives. All image exposure settings were kept consistent across genotypes. Fluorescent intensity was quantified using Image J (NIH). Quantification was performed on 18 images per strain, unless otherwise noted. Specifically, 3 representative 40x images were taken from 2 decellularized scaffolds per animal for a total of 6 images per animal.

**Antibodies.** Primary antibodies used for immunoblotting and immunostaining: anti-annexin A6 (cat# ab199422; Abcam), anti-annexin A2 (cat# 610068; BD Bioscience), anti-collagen type 1 (cat# CL50151AP1; Cedarlane), anti-decorin (cat# AF1060; R&D Systems), anti-HSP90 (cat#4874; Cell Signaling Technologies), anti-laminin-2 (α-2 Chain) (cat# L0663; MilliporeSigma), anti-MMP9 (cat# ab38898; Abcam), anti-periostin/OSF-2 (cat# NBP130042; Novus Bio), anti-TGF Beta 1 (cat# 218981AP; Proteintech and cat# MA515065; Invitrogen), anti-Thrombospondin-4 (cat# AF2390; R&D Systems), and anti-TIMP-1 (cat# AF980; R&D Systems). Secondary antibodies used: Alexa Fluor 488 goat anti-rat (cat# A11006; Invitrogen), Alexa Fluor 594 goat anti-rabbit (cat# A11012; Invitrogen) and Alexa Fluor 594 donkey anti-goat (cat# A11058; Invitrogen).

**Statistical Analyses.** Statistical analyses were performed with Prism (GraphPad, La Jolla, CA). Comparisons relied on 1-way ANOVA for 1 variable or 2-way ANOVA for two variables. Otherwise, unpaired two-tailed t-tests were performed. A p-value less than or equal to 0.05 was considered significant. Data were presented as single values were appropriate. Error bars represent +/- standard error of the mean (SEM).

## AUTHOR CONTRIBTUITIONS

AL, JK, NR, JO, GL and AD prepared dECM and performed immunofluorescence imaging. AL and AD quantified the fluorescence images. MH performed mouse husbandry. AL, NR and LV performed the muscle isolations and related immunoblots. PP performed histological stains. RC and JR provided dECM methodology and critical input in experimental design. AL, AD and EM conceived and designed the studies, analyzed the data, and wrote the manuscript.

**ACKNOWLEDGEMENTS**

This work was supported by National Institutes of Health NS047726, AR052646, HL061322, R01AR048179, and T32AR065972. Additional funding was through Lakeside Discovery. We acknowledge the Jain Foundation for providing dysferlin-null mice from their private colony at The Jackson Laboratory.

## CONFLICT OF INTEREST

Northwestern University filed provisional patents #62/783,619 and #63/309,925 on behalf of the authors (ARD and EMM). The other authors have declared that no conflict of interest exists.

## REFERENCES


Bansal, D., K. Miyake, S.S. Vogel, S. Groh, C.C. Chen, R. Williamson, P.L. McNeil, and K.P. Campbell. 2003. Defective membrane repair in dysferlin-deficient muscular dystrophy. *Nature*. 423:168-172.

Baptista, P.M., M.M. Siddiqui, G. Lozier, S.R. Rodriguez, A. Atala, and S. Soker. 2011. The use of whole organ decellularization for the generation of a vascularized liver organoid. *Hepatology*. 53:604-617.

Bashir, R., S. Britton, T. Strachan, S. Keers, E. Vafiadaki, M. Lako, I. Richard, S. Marchand, N. Bourg, Z. Argov, M. Sadeh, I. Mahjneh, G. Marconi, M.R. Passos-Bueno, S. Moreira Ede, M. Zatz, J.S. Beckmann, and K. Bushby. 1998. A gene related to Caenorhabditis elegans spermatogenesis factor fer-1 is mutated in limb-girdle muscular dystrophy type 2B. *Nat Genet*. 20:37-42.

Belvedere, R., V. Bizzarro, A. Popolo, F. Dal Piaz, M. Vasaturo, P. Picardi, L. Parente, and A. Petrella. 2014. Role of intracellular and extracellular annexin A1 in migration and invasion of human pancreatic carcinoma cells. *BMC Cancer*. 14:961.

Bizzarro, V., R. Belvedere, F. Dal Piaz, L. Parente, and A. Petrella. 2012. Annexin A1 induces skeletal muscle cell migration acting through formyl peptide receptors. *PLoS One*. 7:e48246.

Bonnemann, C.G., C.H. Wang, S. Quijano-Roy, N. Deconinck, E. Bertini, A. Ferreiro, F. Muntoni, C. Sewry, C. Beroud, K.D. Mathews, S.A. Moore, J. Bellini, A. Rutkowski, K.N. North, and D. Members of International Standard of Care Committee for Congenital Muscular. 2014. Diagnostic approach to the congenital muscular dystrophies. *Neuromuscul Disord*. 24:289-311.

Boye, T.L., J.C. Jeppesen, K. Maeda, W. Pezeshkian, V. Solovyeva, J. Nylandsted, and A.C. Simonsen. 2018. Annexins induce curvature on free-edge membranes displaying distinct morphologies. *Scientific Reports*. 8:10309.

Boye, T.L., K. Maeda, W. Pezeshkian, S.L. Sonder, S.C. Haeger, V. Gerke, A.C. Simonsen, and J. Nylandsted. 2017. Annexin A4 and A6 induce membrane curvature and constriction during cell membrane repair. *Nat Commun*. 8:1623.

Brody, M.J., D. Vanhoutte, T.G. Schips, J.G. Boyer, C.V. Bakshi, M.A. Sargent, A.J. York, and J.D. Molkentin. 2018. Defective Flux of Thrombospondin-4 through the Secretory Pathway Impairs Cardiomyocyte Membrane Stability and Causes Cardiomyopathy. *Mol Cell Biol*. 38.

Caceres, S., C. Cuellar, J.C. Casar, J. Garrido, L. Schaefer, H. Kresse, and E. Brandan. 2000. Synthesis of proteoglycans is augmented in dystrophic mdx mouse skeletal muscle. *Eur J Cell Biol*. 79:173-181.

Campbell, K.P., and S.D. Kahl. 1989. Association of dystrophin and an integral membrane glycoprotein. *Nature*. 338:259-262.

Capote, J., I. Kramerova, L. Martinez, S. Vetrone, E.R. Barton, H.L. Sweeney, M.C. Miceli, and M.J. Spencer. 2016. Osteopontin ablation ameliorates muscular dystrophy by shifting macrophages to a pro-regenerative phenotype. *J Cell Biol*. 213:275-288.

Ceco, E., S. Bogdanovich, B. Gardner, T. Miller, A. DeJesus, J.U. Earley, M. Hadhazy, L.R. Smith, E.R. Barton, J.D. Molkentin, and E.M. McNally. 2014. Targeting latent TGFbeta release in muscular dystrophy. *Sci Transl Med*. 6:259ra144.

Chen, X., and Y. Li. 2009. Role of matrix metalloproteinases in skeletal muscle: migration, differentiation, regeneration and fibrosis. *Cell Adh Migr*. 3:337-341.

Chen, Y.W., P. Zhao, R. Borup, and E.P. Hoffman. 2000. Expression profiling in the muscular dystrophies: identification of novel aspects of molecular pathophysiology. *J Cell Biol*. 151:1321-1336.

Coley, W.D., L. Bogdanik, M.C. Vila, Q. Yu, J.H. Van Der Meulen, S. Rayavarapu, J.S. Novak, M. Nearing, J.L. Quinn, A. Saunders, C. Dolan, W. Andrews, C. Lammert, A. Austin, T.A. Partridge, G.A. Cox, C. Lutz, and K. Nagaraju. 2016. Effect of genetic background on the dystrophic phenotype in mdx mice. *Hum Mol Genet*. 25:130-145.

Contreras-Cubas, C., F. Barajas-Olmos, M.I. Frayre-Martinez, G. Siordia-Reyes, C.C. Guizar-Sanchez, H. Garcia-Ortiz, L. Orozco, and V. Baca. 2022. Dysferlinopathy misdiagnosed with juvenile polymyositis in the pre-symptomatic stage of hyperCKemia: a case report and literature review. *BMC Med Genomics*. 15:139.

Crapo, P.M., T.W. Gilbert, and S.F. Badylak. 2011. An overview of tissue and whole organ decellularization processes. *Biomaterials*. 32:3233-3243.

Croissant, C., C. Gounou, F. Bouvet, S. Tan, and A. Bouter. 2020. Annexin-A6 in Membrane Repair of Human Skeletal Muscle Cell: A Role in the Cap Subdomain. *Cells*. 9.

Dadgar, S., Z. Wang, H. Johnston, A. Kesari, K. Nagaraju, Y.W. Chen, D.A. Hill, T.A. Partridge, M. Giri, R.J. Freishtat, J. Nazarian, J. Xuan, Y. Wang, and E.P. Hoffman. 2014. Asynchronous remodeling is a driver of failed regeneration in Duchenne muscular dystrophy. *J Cell Biol*. 207:139-158.

Davis, D.B., K.R. Doherty, A.J. Delmonte, and E.M. McNally. 2002. Calcium-sensitive phospholipid binding properties of normal and mutant ferlin C2 domains. *J Biol Chem*. 277:22883-22888.

Defour, A., J.H. Van der Meulen, R. Bhat, A. Bigot, R. Bashir, K. Nagaraju, and J.K. Jaiswal. 2014. Dysferlin regulates cell membrane repair by facilitating injury-triggered acid sphingomyelinase secretion. *Cell Death Dis*. 5:e1306.

Demonbreun, A.R., E. Bogdanovic, L.A. Vaught, N.L. Reiser, K.S. Fallon, A.M. Long, C.C. Oosterbaan, M. Hadhazy, P.G. Page, P.R.B. Joseph, G. Cowen, A.M. Telenson, A. Khatri, K.R. Sadleir, R. Vassar, and E.M. McNally. 2022. A conserved annexin A6-mediated membrane repair mechanism in muscle, heart, and nerve. *JCI Insight*. 7.

Demonbreun, A.R., K.S. Fallon, C.C. Oosterbaan, E. Bogdanovic, J.L. Warner, J.J. Sell, P.G. Page, M. Quattrocelli, D.Y. Barefield, and E.M. McNally. 2019a. Recombinant annexin A6 promotes membrane repair and protects against muscle injury. *J Clin Invest*. 129:4657-4670.

Demonbreun, A.R., M. Quattrocelli, D.Y. Barefield, M.V. Allen, K.E. Swanson, and E.M. McNally. 2016. An actin-dependent annexin complex mediates plasma membrane repair in muscle. *J Cell Biol*. 213:705-718.

Demonbreun, A.R., E.J. Wyatt, K.S. Fallon, C.C. Oosterbaan, P.G. Page, M. Hadhazy, M. Quattrocelli, D.Y. Barefield, and E.M. McNally. 2019b. A gene-edited mouse model of limb-girdle muscular dystrophy 2C for testing exon skipping. *Dis Model Mech*. 13.

Dowling, P., S. Gargan, S. Murphy, M. Zweyer, H. Sabir, D. Swandulla, and K. Ohlendieck. 2021. The Dystrophin Node as Integrator of Cytoskeletal Organization, Lateral Force Transmission, Fiber Stability and Cellular Signaling in Skeletal Muscle. *Proteomes*. 9.

Fadic, R., V. Mezzano, K. Alvarez, D. Cabrera, J. Holmgren, and E. Brandan. 2006. Increase in decorin and biglycan in Duchenne Muscular Dystrophy: role of fibroblasts as cell source of these proteoglycans in the disease. *J Cell Mol Med*. 10:758-769.

Flanigan, K.M., E. Ceco, K.M. Lamar, Y. Kaminoh, D.M. Dunn, J.R. Mendell, W.M. King, A. Pestronk, J.M. Florence, K.D. Mathews, R.S. Finkel, K.J. Swoboda, E. Gappmaier, M.T. Howard, J.W. Day, C. McDonald, E.M. McNally, R.B. Weiss, and P. United Dystrophinopathy. 2013. LTBP4 genotype predicts age of ambulatory loss in Duchenne muscular dystrophy. *Ann Neurol*. 73:481-488.

Garcia-Melero, A., M. Reverter, M. Hoque, E. Meneses-Salas, M. Koese, J.R. Conway, C.H. Johnsen, A. Alvarez-Guaita, F. Morales-Paytuvi, Y.A. Elmaghrabi, A. Pol, F. Tebar, R.Z. Murray, P. Timpson, C. Enrich, T. Grewal, and C. Rentero. 2016. Annexin A6 and Late

Endosomal Cholesterol Modulate Integrin Recycling and Cell Migration. *J Biol Chem*. 291:1320-1335.
Gilpin, A., and Y. Yang. 2017. Decellularization Strategies for Regenerative Medicine: From Processing Techniques to Applications. *Biomed Res Int*. 2017:9831534.
Gordish-Dressman, H., R. Willmann, L. Dalle Pazze, A. Kreibich, M. van Putten, A. Heydemann, L. Bogdanik, C. Lutz, K. Davies, A.R. Demonbreun, D. Duan, D. Elsey, S.I. Fukada, M. Girgenrath, J. Patrick Gonzalez, M.D. Grounds, A. Nichols, T. Partridge, M. Passini, F. Sanarica, F.J. Schnell, D.J. Wells, T. Yokota, C.S. Young, Z. Zhong, C. Spurney, M. Spencer, A. De Luca, K. Nagaraju, and A. Aartsma-Rus. 2018. "Of Mice and Measures": A Project to Improve How We Advance Duchenne Muscular Dystrophy Therapies to the Clinic. *J Neuromuscul Dis*. 5:407-417.
Grewal, T., M. Hoque, J.R.W. Conway, M. Reverter, M. Wahba, S.S. Beevi, P. Timpson, C. Enrich, and C. Rentero. 2017. Annexin A6-A multifunctional scaffold in cell motility. *Cell Adh Migr*. 11:288-304.
Hack, A.A., C.T. Ly, F. Jiang, C.J. Clendenin, K.S. Sigrist, R.L. Wollmann, and E.M. McNally. 1998. Gamma-sarcoglycan deficiency leads to muscle membrane defects and apoptosis independent of dystrophin. *J Cell Biol*. 142:1279-1287.
Hakkinen, K.M., J.S. Harunaga, A.D. Doyle, and K.M. Yamada. 2011. Direct comparisons of the morphology, migration, cell adhesions, and actin cytoskeleton of fibroblasts in four different three-dimensional extracellular matrices. *Tissue Eng Part A*. 17:713-724.
Hammers, D.W., C.C. Hart, M.K. Matheny, L.A. Wright, M. Armellini, E.R. Barton, and H.L. Sweeney. 2020. The D2.mdx mouse as a preclinical model of the skeletal muscle pathology associated with Duchenne muscular dystrophy. *Sci Rep*. 10:14070.
Han, R., E.P. Rader, J.R. Levy, D. Bansal, and K.P. Campbell. 2011. Dystrophin deficiency exacerbates skeletal muscle pathology in dysferlin-null mice. *Skelet Muscle*. 1:35.
Harris, G.M., I. Raitman, and J.E. Schwarzbauer. 2018. Cell-derived decellularized extracellular matrices. *Methods Cell Biol*. 143:97-114.
Heydemann, A., E. Ceco, J.E. Lim, M. Hadhazy, P. Ryder, J.L. Moran, D.R. Beier, A.A. Palmer, and E.M. McNally. 2009. Latent TGF-beta-binding protein 4 modifies muscular dystrophy in mice. *J Clin Invest*. 119:3703-3712.
Heydemann, A., J.M. Huber, A. Demonbreun, M. Hadhazy, and E.M. McNally. 2005. Genetic background influences muscular dystrophy. *Neuromuscul Disord*. 15:601-609.
Ho, M., C.M. Post, L.R. Donahue, H.G. Lidov, R.T. Bronson, H. Goolsby, S.C. Watkins, G.A. Cox, and R.H. Brown, Jr. 2004. Disruption of muscle membrane and phenotype divergence in two novel mouse models of dysferlin deficiency. *Hum Mol Genet*. 13:1999-2010.
Hogarth, M.W., A. Defour, C. Lazarski, E. Gallardo, J. Diaz Manera, T.A. Partridge, K. Nagaraju, and J.K. Jaiswal. 2019. Fibroadipogenic progenitors are responsible for muscle loss in limb girdle muscular dystrophy 2B. *Nat Commun*. 10:2430.
Hoshiba, T. 2019. Decellularized Extracellular Matrix for Cancer Research. *Materials (Basel)*. 12.
Hussein, K.H., K.M. Park, J.H. Ghim, S.R. Yang, and H.M. Woo. 2016. Three dimensional culture of HepG2 liver cells on a rat decellularized liver matrix for pharmacological studies. *J Biomed Mater Res B Appl Biomater*. 104:263-273.
Iqbal, A., U. May, S.N. Prince, T.A.H. Jarvinen, and A. Heydemann. 2021. Systemically Administered Homing Peptide Targets Dystrophic Lesions and Delivers Transforming Growth Factor-beta (TGFbeta) Inhibitor to Attenuate Murine Muscular Dystrophy Pathology. *Pharmaceutics*. 13.
Kramerova, I., C. Kumagai-Cresse, N. Ermolova, E. Mokhonova, M. Marinov, J. Capote, D. Becerra, M. Quattrocelli, R.H. Crosbie, E. Welch, E.M. McNally, and M.J. Spencer. 2019.

Spp1 (osteopontin) promotes TGFbeta processing in fibroblasts of dystrophin-deficient muscles through matrix metalloproteinases. *Hum Mol Genet*. 28:3431-3442.
Lek, A., F.J. Evesson, R.B. Sutton, K.N. North, and S.T. Cooper. 2012. Ferlins: regulators of vesicle fusion for auditory neurotransmission, receptor trafficking and membrane repair. *Traffic*. 13:185-194.
Li, Y., J. Li, J. Zhu, B. Sun, M. Branca, Y. Tang, W. Foster, X. Xiao, and J. Huard. 2007. Decorin gene transfer promotes muscle cell differentiation and muscle regeneration. *Mol Ther*. 15:1616-1622.
Lim, L.E., F. Duclos, O. Broux, N. Bourg, Y. Sunada, V. Allamand, J. Meyer, I. Richard, C. Moomaw, C. Slaughter, and et al. 1995. Beta-sarcoglycan: characterization and role in limb-girdle muscular dystrophy linked to 4q12. *Nat Genet*. 11:257-265.
Liu, J., M. Aoki, I. Illa, C. Wu, M. Fardeau, C. Angelini, C. Serrano, J.A. Urtizberea, F. Hentati, M.B. Hamida, S. Bohlega, E.J. Culper, A.A. Amato, K. Bossie, J. Oeltjen, K. Bejaoui, D. McKenna-Yasek, B.A. Hosler, E. Schurr, K. Arahata, P.J. de Jong, and R.H. Brown, Jr. 1998. Dysferlin, a novel skeletal muscle gene, is mutated in Miyoshi myopathy and limb girdle muscular dystrophy. *Nat Genet*. 20:31-36.
Loreti, M., and A. Sacco. 2022. The jam session between muscle stem cells and the extracellular matrix in the tissue microenvironment. *NPJ Regen Med*. 7:16.
Lorts, A., J.A. Schwanekamp, T.A. Baudino, E.M. McNally, and J.D. Molkentin. 2012. Deletion of periostin reduces muscular dystrophy and fibrosis in mice by modulating the transforming growth factor-beta pathway. *Proc Natl Acad Sci U S A*. 109:10978-10983.
Lostal, W., M. Bartoli, N. Bourg, C. Roudaut, A. Bentaib, K. Miyake, N. Guerchet, F. Fougerousse, P. McNeil, and I. Richard. 2010. Efficient recovery of dysferlin deficiency by dual adeno-associated vector-mediated gene transfer. *Hum Mol Genet*. 19:1897-1907.
McDade, J.R., A. Archambeau, and D.E. Michele. 2014. Rapid actin-cytoskeleton-dependent recruitment of plasma membrane-derived dysferlin at wounds is critical for muscle membrane repair. *FASEB J*. 28:3660-3670.
Mendell, J.R., D.R. Boue, and P.T. Martin. 2006. The congenital muscular dystrophies: recent advances and molecular insights. *Pediatr Dev Pathol*. 9:427-443.
Mendibil, U., R. Ruiz-Hernandez, S. Retegi-Carrion, N. Garcia-Urquia, B. Olalde-Graells, and A. Abarrategi. 2020. Tissue-Specific Decellularization Methods: Rationale and Strategies to Achieve Regenerative Compounds. *Int J Mol Sci*. 21.
Meyer, G.A., and R.L. Lieber. 2011. Elucidation of extracellular matrix mechanics from muscle fibers and fiber bundles. *J Biomech*. 44:771-773.
Monaco, A.P., R.L. Neve, C. Colletti-Feener, C.J. Bertelson, D.M. Kurnit, and L.M. Kunkel. 1986. Isolation of candidate cDNAs for portions of the Duchenne muscular dystrophy gene. *Nature*. 323:646-650.
Naba, A., K.R. Clauser, H. Ding, C.A. Whittaker, S.A. Carr, and R.O. Hynes. 2016. The extracellular matrix: Tools and insights for the “omics” era. *Matrix Biology*. 49:10-24.
Naba, A., K.R. Clauser, S. Hoersch, H. Liu, S.A. Carr, and R.O. Hynes. 2012. The matrisome: in silico definition and in vivo characterization by proteomics of normal and tumor extracellular matrices. *Mol Cell Proteomics*. 11:M111 014647.
Nigro, V., E. de Sa Moreira, G. Piluso, M. Vainzof, A. Belsito, L. Politano, A.A. Puca, M.R. Passos-Bueno, and M. Zatz. 1996. Autosomal recessive limb-girdle muscular dystrophy, LGMD2F, is caused by a mutation in the delta-sarcoglycan gene. *Nat Genet*. 14:195-198.
Noguchi, S., E.M. McNally, K. Ben Othmane, Y. Hagiwara, Y. Mizuno, M. Yoshida, H. Yamamoto, C.G. Bonnemann, E. Gussoni, P.H. Denton, T. Kyriakides, L. Middleton, F. Hentati, M. Ben Hamida, I. Nonaka, J.M. Vance, L.M. Kunkel, and E. Ozawa. 1995.

Mutations in the dystrophin-associated protein gamma-sarcoglycan in chromosome 13 muscular dystrophy. *Science*. 270:819-822.
Pegoraro, E., E.P. Hoffman, L. Piva, B.F. Gavassini, S. Cagnin, M. Ermani, L. Bello, G. Soraru, B. Pacchioni, M.D. Bonifati, G. Lanfranchi, C. Angelini, A. Kesari, I. Lee, H. Gordish-Dressman, J.M. Devaney, C.M. McDonald, and G. Cooperative International Neuromuscular Research. 2011. SPP1 genotype is a determinant of disease severity in Duchenne muscular dystrophy. *Neurology*. 76:219-226.
Rando, T.A. 2001. The dystrophin-glycoprotein complex, cellular signaling, and the regulation of cell survival in the muscular dystrophies. *Muscle Nerve*. 24:1575-1594.
Roman, W., H. Pinheiro, M.R. Pimentel, J. Segales, L.M. Oliveira, E. Garcia-Dominguez, M.C. Gomez-Cabrera, A.L. Serrano, E.R. Gomes, and P. Munoz-Canoves. 2021. Muscle repair after physiological damage relies on nuclear migration for cellular reconstruction. *Science*. 374:355-359.
Roostalu, U., and U. Strahle. 2012. In vivo imaging of molecular interactions at damaged sarcolemma. *Dev Cell*. 22:515-529.
Shao, X., I.N. Taha, K.R. Clauser, Y. Gao, and A. Naba. 2019. MatrisomeDB: the ECM-protein knowledge database. *Nucleic Acids Research*. 48:D1136-D1144.
Sicinski, P., Y. Geng, A.S. Ryder-Cook, E.A. Barnard, M.G. Darlison, and P.J. Barnard. 1989. The molecular basis of muscular dystrophy in the mdx mouse: a point mutation. *Science*. 244:1578-1580.
Snider, P., R.B. Hinton, R.A. Moreno-Rodriguez, J. Wang, R. Rogers, A. Lindsley, F. Li, D.A. Ingram, D. Menick, L. Field, A.B. Firulli, J.D. Molkentin, R. Markwald, and S.J. Conway. 2008. Periostin is required for maturation and extracellular matrix stabilization of noncardiomyocyte lineages of the heart. *Circ Res*. 102:752-760.
Stearns-Reider, K.M., M.R. Hicks, K.G. Hammond, J.C. Reynolds, A. Maity, Y.Z. Kurmangaliyev, J. Chin, A. Stieg, N.A. Geisse, S. Hohlbauch, S. Kaemmer, L.R. Schmitt, T.T. Pham, K. Yamauchi, B.G. Novitch, R. Wollman, K.C. Hansen, A.D. Pyle, and R.H. Crosbie. 2022. Myoscaffolds reveal laminin scarring is detrimental for stem cell function while sarcospan induces compensatory fibrosis. *bioRxiv*:2022.2007.2007.497559.
Subramanian, A., and T.F. Schilling. 2014. Thrombospondin-4 controls matrix assembly during development and repair of myotendinous junctions. *Elife*. 3.
Swaggart, K.A., A.R. Demonbreun, A.H. Vo, K.E. Swanson, E.Y. Kim, J.P. Fahrenbach, J. Holley-Cuthrell, A. Eskin, Z. Chen, K. Squire, A. Heydemann, A.A. Palmer, S.F. Nelson, and E.M. McNally. 2014. Annexin A6 modifies muscular dystrophy by mediating sarcolemmal repair. *Proc Natl Acad Sci U S A*. 111:6004-6009.
Tan, Y.H., H.R. Helms, and K.H. Nakayama. 2022. Decellularization Strategies for Regenerating Cardiac and Skeletal Muscle Tissues. *Front Bioeng Biotechnol*. 10:831300.
Thomas, K., A.J. Engler, and G.A. Meyer. 2015. Extracellular matrix regulation in the muscle satellite cell niche. *Connect Tissue Res*. 56:1-8.
van Putten, M., E.M. Lloyd, J.C. de Greef, V. Raz, R. Willmann, and M.D. Grounds. 2020. Mouse models for muscular dystrophies: an overview. *Dis Model Mech*. 13.
Vanhoutte, D., T.G. Schips, J.Q. Kwong, J. Davis, A. Tjondrokoesoemo, M.J. Brody, M.A. Sargent, O. Kanisicak, H. Yi, Q.Q. Gao, J.E. Rabinowitz, T. Volk, E.M. McNally, and J.D. Molkentin. 2016. Thrombospondin expression in myofibers stabilizes muscle membranes. *Elife*. 5.
Zanotti, S., T. Negri, C. Cappelletti, P. Bernasconi, E. Canioni, C. Di Blasi, E. Pegoraro, C. Angelini, P. Ciscato, A. Prelle, R. Mantegazza, L. Morandi, and M. Mora. 2005. Decorin and biglycan expression is differentially altered in several muscular dystrophies. *Brain*. 128:2546-2555.

**TABLE 1. Muscular dystrophy mouse models used in this study.**

| Mouse Model | Human Disease | Protein Affected | Background Strain | Genetic Mutation | Dystrophy Phenotype | References |
|---|---|---|---|---|---|---|
| *mdx* | DMD | dystrophin | C57BL/10 | Premature stop C>T; p.Q995* exon 23 *Dmd* | mild | Sicinski et al., 1989 |
| *mdxD2* | DMD | dystrophin | DBA2/J | Premature stop C>T; p.Q995* exon 23 *Dmd* | severe | Coley et al., 2016 |
| *Sgcg* | LGMD2C | γ-sarcoglycan | C57BL/6 | Neo insertion Exon 2 *Sgcg* | mild | Hack et al., 1998 |
| *SgcgD2* | LGMD2C | γ-sarcoglycan | DBA2/J | 521dT deletion exon 6 *Sgcg* | severe | Demonbreun et al., 2019b |
| *BLAJ* | LGMD2B MM | dysferlin | C57BL/6 | Retrotransposon insertion intron 4 *Dysf* | mild | Ho et al., 2004 Lostal et al., 2010 |
| *mdx hLTBP4* | DMD | dystrophin | C57BL/6 | Human LTBP4 Bac Transgene | moderate | Ceco et al., 2014 |

## FIGURES AND LEGENDS

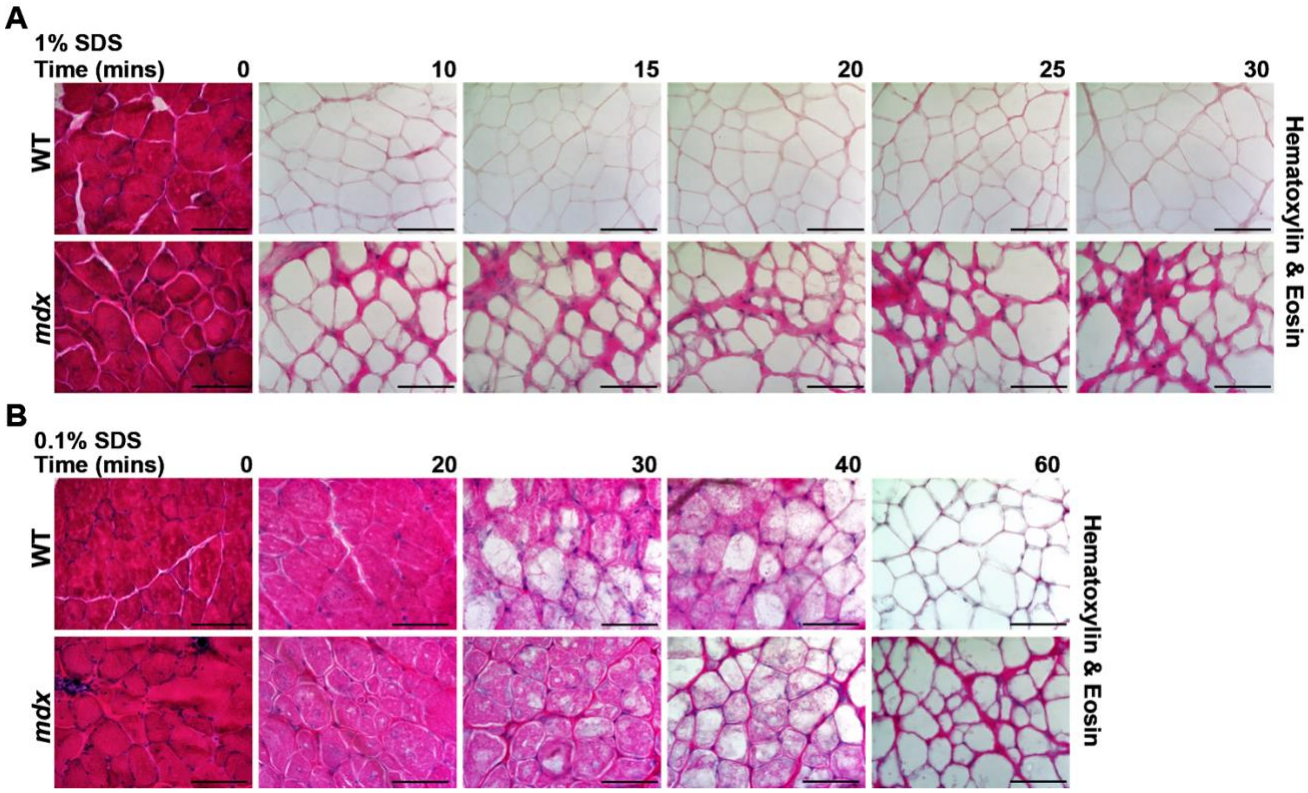


**Figure 1. Ten-minute incubation with 1% SDS resulted in optimal on-slide decellularization of skeletal muscle sections.** Representative images of Hematoxylin & Eosin (H&E) staining of wild-type (WT) and *mdx* quadriceps muscles that were decellularized with 1% SDS or 0.1% SDS for the labeled times (10 to 60 minutes). Non-decellularized sections, treated with PBS only, were served as controls (0 minutes). (**A**) Exposure of slides to 1% SDS solution produced complete decellularization of the myoscaffolds after 10 minutes. (**B**) At 0.1% SDS, longer incubation times are needed for decellularization, with total loss of cellular components achieved at 60 minutes. Scale bars are set at 100μm.

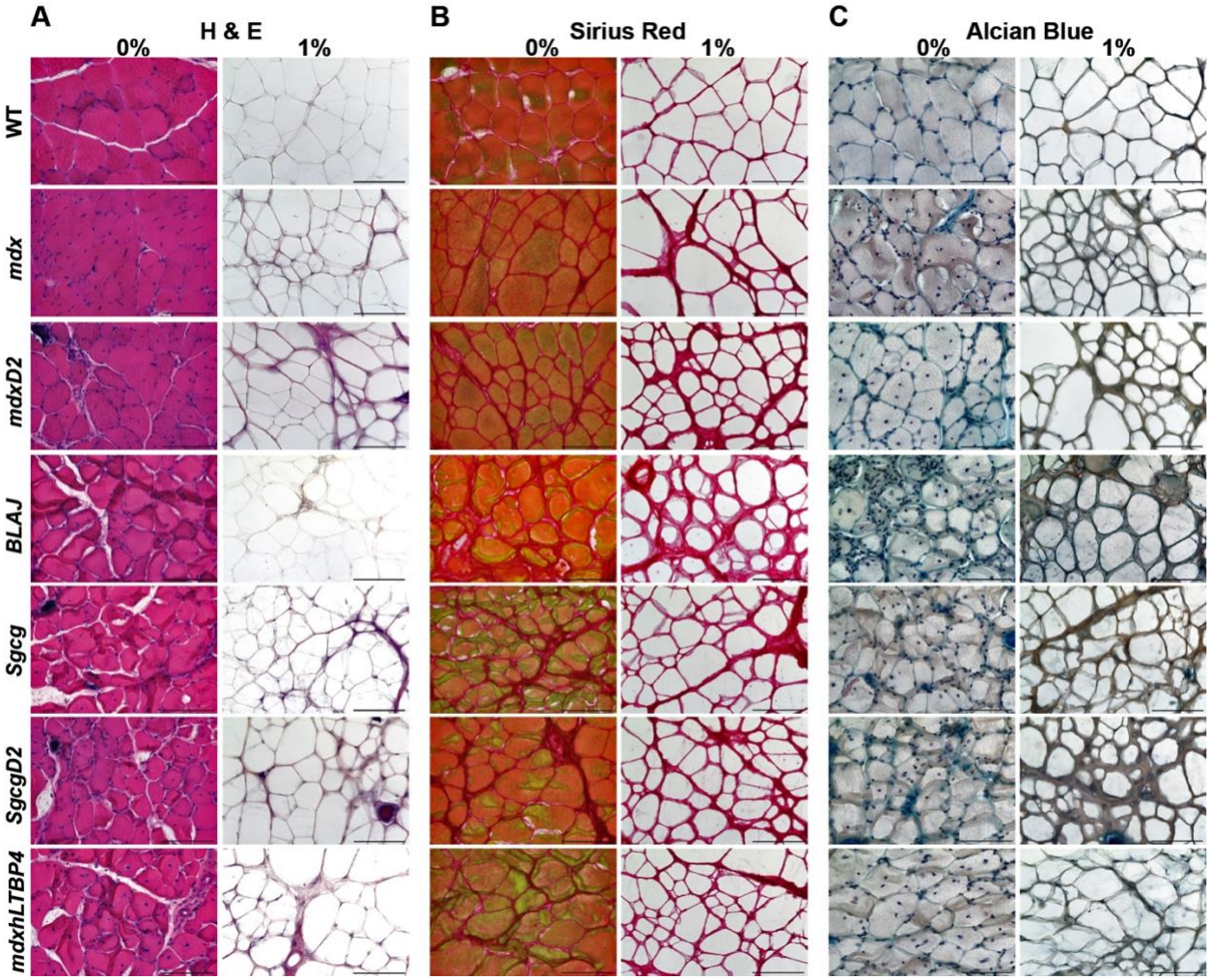


**Figure 2. Acellular myoscaffolds retained ECM architectural integrity and glycosaminoglycans after on-slide decellularization.** Muscle sections from WT and multiple muscular dystrophy mouse models including *mdx*, *mdxD2*, *BLAJ*, *Sgcg*, *SgcgD2*, and *mdxhLTBP4*) were decellularized with a 1% SDS solution (1%) for 10 minutes. The non-decellularized control was incubated in PBS (0%). Representative images of (**A**) H&E, (**B**) Sirius Red, and (**C**) Alcian Blue staining demonstrate complete removal of cellular components, preservation of the dECM collagen structure and retention of glycosaminoglycans respectively. Scale bars are set at 100μm; n=3 independent mice per strain.

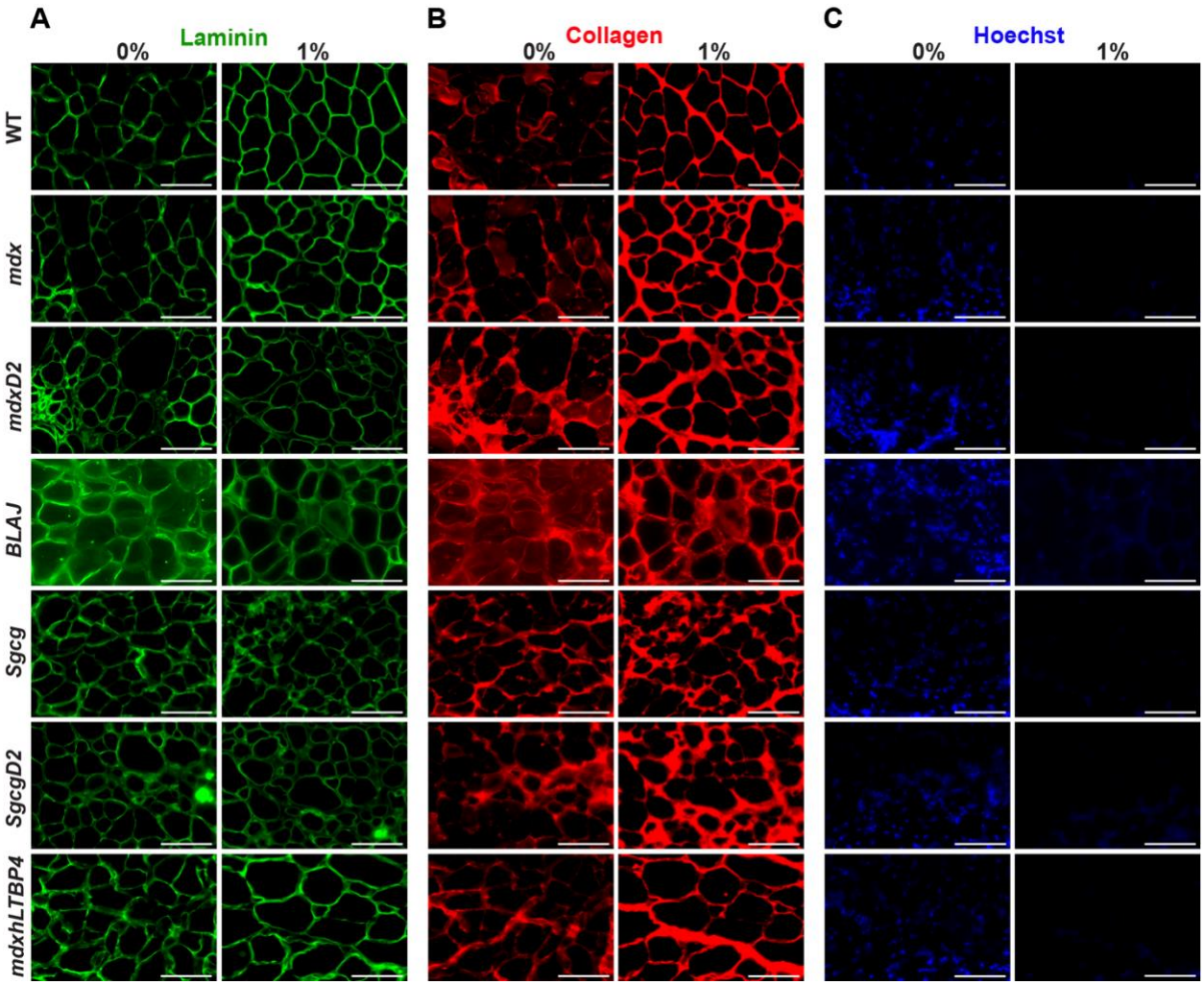


**Figure 3. Acellular myoscaffolds from dystrophic models demonstrated excess collagen deposition in all models.** Immunofluorescence microscopy (IFM) was performed on decellularized (1%) myoscaffolds from WT and muscular dystrophy mouse models (*mdx*, *mdxD2*, *BLAJ*, *Sgcg*, *SgcgD2*, and *mdxhLTBP4*). PBS was used for a non-decellularized control (0%). Representative images of (**A**) Laminin, (**B**) Collagen I, and (**C**) Hoechst staining demonstrate intact ECM structure, increased collagen deposition within more fibrotic matrices, and removal of cellular DNA respectively. Scale bars are set at 100μm; n=3 independent mice per strain.

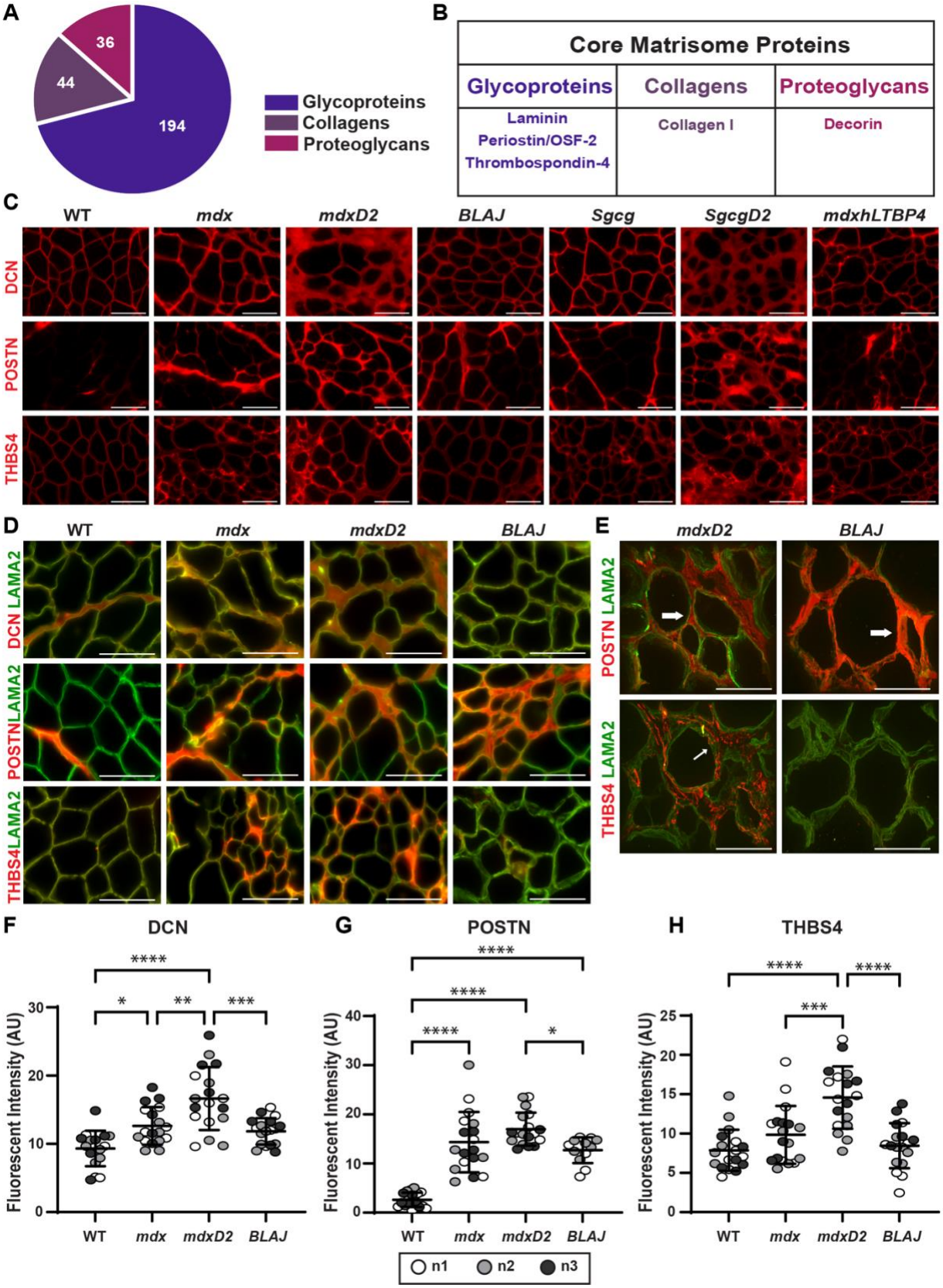
A
36
44
194
Glycoproteins
Collagens
Proteoglycans
B
Core Matrisome Proteins
Glycoproteins
Collagens
Proteoglycans
Laminin
Periostin/OSF-2
Thrombospondin-4
Collagen I
Decorin
C
WT
mdx
mdxD2
BLAJ
Sgcg
SgcgD2
mdxhLTBP4
DCN
POSTN
THBS4
D
WT
mdx
mdxD2
BLAJ
DCN LAMA2
POSTN LAMA2
THBS4 LAMA2
E
mdxD2
BLAJ
POSTN LAMA2
THBS4 LAMA2
F
DCN
Fluorescent Intensity (AU)
WT
mdx
mdxD2
BLAJ
G
POSTN
H
THBS4
n1
n2
n3

**Figure 4. Acellular myoscaffolds differentially retained core matrisome proteins decorin, periostin and thrombospondin 4 in different muscular dystrophy models**. (**A**) Schematic pie chart showing protein categories and totals included under the Core Matrisome Proteins heading as defined by Naba et al 2012 (Naba et al., 2012). (**B**) Proteins analyzed in this study. (**C**) Representative IFM images from acellular myoscaffolds from WT and *mdx*, *mdxD2*, *BLAJ*, *Sgcg*, *SgcgD2*, and *mdxhLTBP4*. The dECMs were stained with antibodies against decorin (DCN), periostin (POSTN), or thrombospondin-4 (THBS4). (**D**) Representative IFM performed on the dECMs of WT, *mdx*, *mdxD2*, and *BLAJ* of DCN, POSTN, or THBS4 (red) overlayed with laminin (green) demonstrate that DCN was observed diffusely throughout the muscle in dystrophic muscles from the DBA/2J background (*mdxD2*, *SgcgD2*). POSTN was increased in all muscular dystrophy subtypes but in a non-uniform manner across each muscle. THBS4 protein expression was more focally upregulated in specific regions of the myoscaffolds, and like DCN, was greatest in the DBA/2J background muscular dystrophy models. All scale bars are set at 100μm. (**E**) 100x Z-stack representative images of POSTN or THBS4 (red) overlayed on laminin (green) demonstrate unique protein deposition profiles on the acellular myoscaffolds THBS4 was observed in the matrix in a vesicle-like pattern (thin white arrow), while POSTN was observed in a more diffuse pattern (thick white arrows). Scale bars are set at 50μm. IFM quantification demonstrate a significant increase in mean fluorescent intensity in myoscaffolds (**F**) DCN (WT 9.7, *mdx* 13.2, *mdxD2* 17.3, *BLAJ* 12.3 AU), (**G**) POSTN (WT 2.6, *mdx* 14.3, *mdxD2* 17.0, *BLAJ* 12.7 AU), and (**H**) THBS4 (WT 7.8, *mdx* 9.8, *mdxD2* 14.6, *BLAJ* 8.5 AU). n=3 independent mice per strain (marked as n1, n2, n3), n=6 images from 2 scaffolds per mouse. Graphs show the mean with SEM bars. * $p < 0.05$, ** $p < 0.01$, *** $p < 0.005$, and **** $p < 0.001$ by one-way ANOVA.

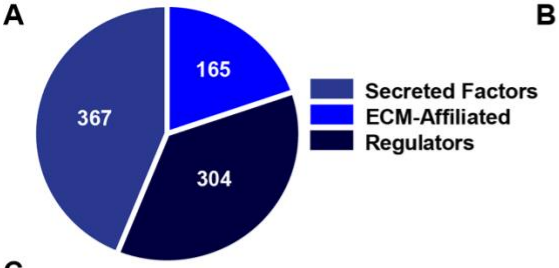


B

| Matrisome-Associated Proteins | | |
|---|---|---|
| ECM-Affiliated | Regulators | Secreted Factors |
| Annexin A2<br>Annexin A6 | MMP9<br>TIMP1 | TGFB1 |

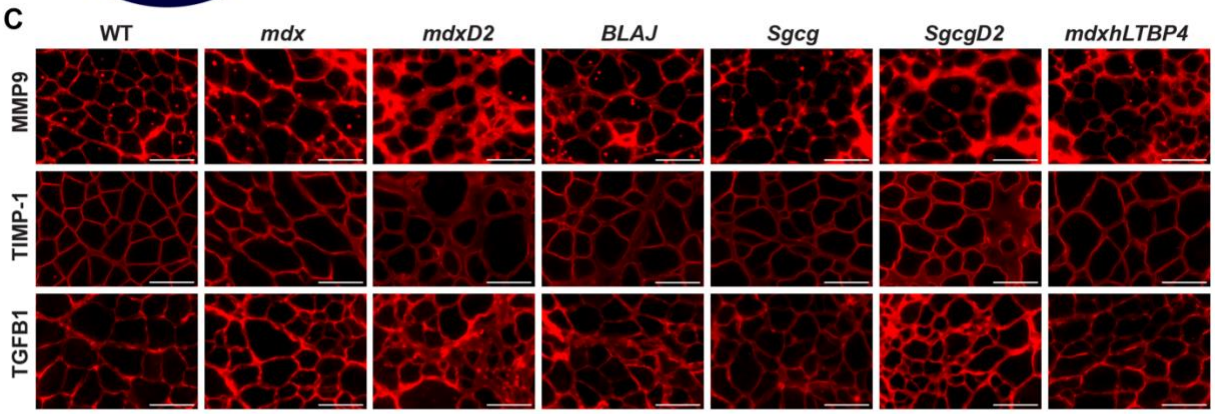


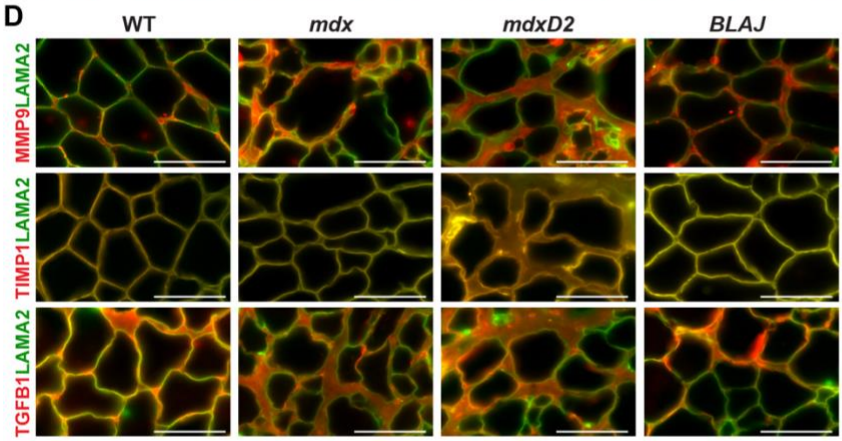


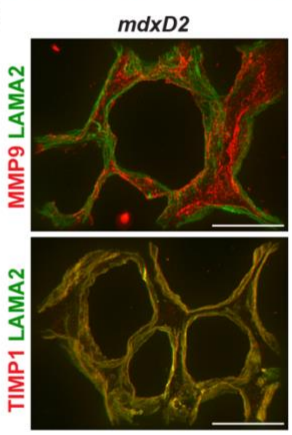


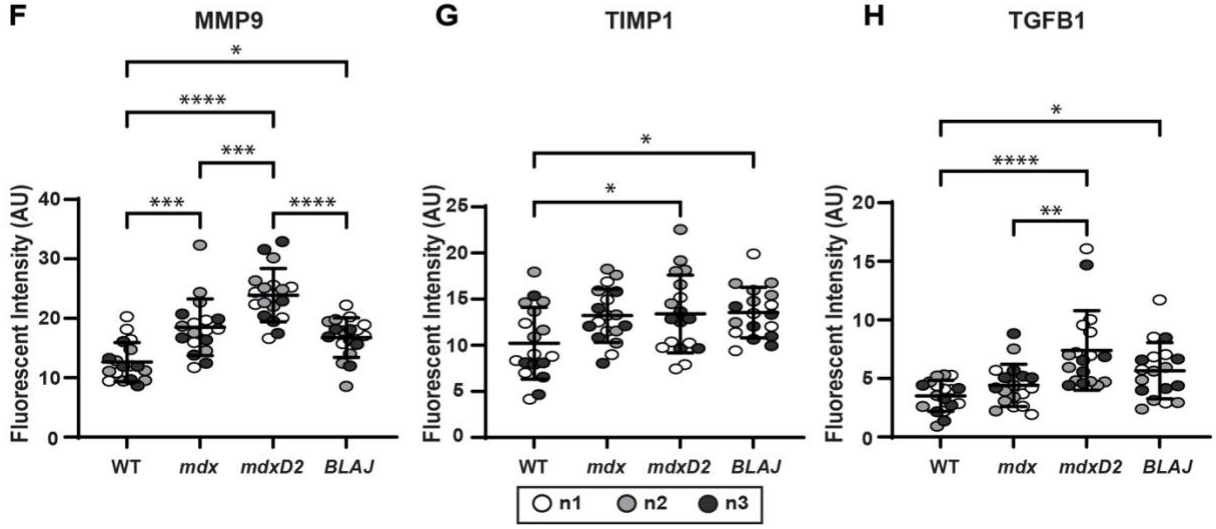

**Figure 5. Acellular myoscaffolds retained matrisome-associated proteins MMP9, TIMP-1, and TGFB-1 and demonstrate differential expression across different dECM models**. (**A**) Schematic pie chart showing protein categories and totals included under the Matrisome-Associated Proteins heading as defined by Naba et al 2012 (Naba et al., 2012). (**B**) Proteins analyzed in this study. (**C**) Representative IFM images from acellular myoscaffolds from WT and *mdx*, *mdxD2*, *BLAJ*, *Sgcg*, *SgcgD2*, and *mdxhLTBP4* evaluated for MMP9, TIMP-1, or TGF-β1. (**D**) High-magnification IFM images of dECMs generated from WT, *mdx*, *mdxD2*, and *BLAJ* muscle stained with anti- MMP9, TIMP-1, or TGF-β1 (red) and laminin (green) demonstrated unique localization patterns across the myoscaffolds. MMP9 and TGF-β1 were increased in muscular dystrophy models from the DBA/2J background. All scale bars are set at 100μm. (**E**) 100x Z-stack representative images of MMP9 (red) and TIMP-1 (red) co-stained with laminin (green) demonstrate differential expression profiles in *mdxD2* with MMP9 deposited on the matrix in vesicle-like pattern and TIMP-1 exhibiting a diffuse ubiquitous expression pattern. Scale bars are set at 50μm. (**F**) MMP9 (WT 12.7, *mdx* 18.5, *mdxD2* 23.9, *BLAJ* 16.8 AU), (**G**) TIMP-1 (WT 10.2, *mdx* 13.2, *mdxD2* 13.4, *BLAJ* 13.6 AU), and (**H**) TGF-β1 (WT 3.5, *mdx* 4.4, *mdxD2* 7.4, *BLAJ* 5.7 AU) mean fluorescent intensity in myoscaffolds. n=3 independent mice per strain (marked as n1, n2, n3), n=6 images from 2 scaffolds per mouse. Graphs show the mean with SEM bars. * $p < 0.05$, ** $p < 0.01$, *** $p < 0.005$, and **** $p < 0.001$ by one-way ANOVA.

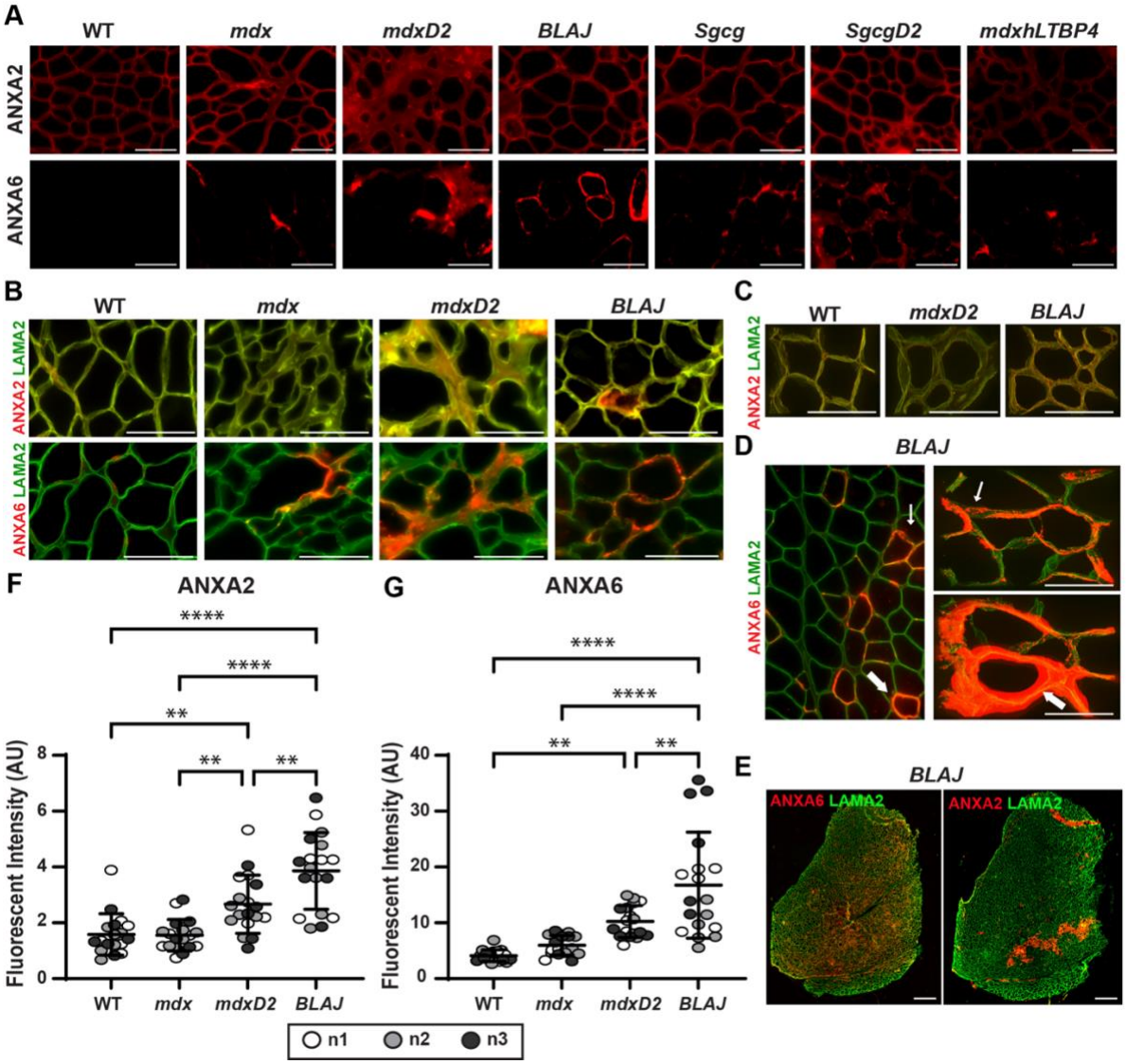


**Figure 6. Excess deposition of annexins in dysferlin deficient myoscaffolds.** (**A**) Representative IFM images from acellular myoscaffolds generated from WT and *mdx*, *mdxD2*, *BLAJ*, *Sgcg*, *SgcgD2*, and *mdxhLTBP4* muscles evaluated for annexin A2 (ANXA2) and annexin A6 (ANXA6). (**B**) ANXA2 and anti-ANXA6 (red) were anti-laminin (green). ANXA2 exhibits a diffuse pattern, while ANXA6 is vesicular. All scale bars are set at 100µm. (**C**) 100x Z-stack images of ANXA2 (red) with laminin co-staining (green) demonstrated diffuse expression on the dECMs generated from WT, *mdxD2* and *BLAJ* muscle. Scale bars 100µm. (**D**) 20x and 100x Z-stack images of ANXA6 illustrated a unique protein deposition profile on *BLAJ* myoscaffolds. ANXA6 (red) appeared in the matrix in a vesicle-like pattern (thin white arrow), which formed a concentrated ring of protein (thick white arrows). Scale bars 100µm. (**E**) Tiled image of a full thickness *BLAJ* dECM scaffold. ANXA6 staining was present throughout the myoscaffold, while ANXA2 staining was concentrated into focal areas. Scale bars 500µm. (**F**) ANXA2 (WT 1.6, *mdx* 1.6, *mdxD2* 2.7, *BLAJ* 3.9 AU) and (**G**) ANXA6 (WT 4.1, *mdx* 6.0, *mdxD2* 10.2, *BLAJ* 16.8 AU) mean fluorescent intensity in myoscaffolds was significantly upregulated in *BLAJ* scaffolds. n=3 independent mice per strain (marked as n1, n2, n3), n=6 images from 2 scaffolds per mouse. Graphs show the mean with SEM bars. * $p < 0.05$, ** $p < 0.01$, *** $p < 0.005$, and **** $p < 0.001$ by one-way ANOVA.

**SUPLLEMENTAL FIGURES AND LEGENDS**

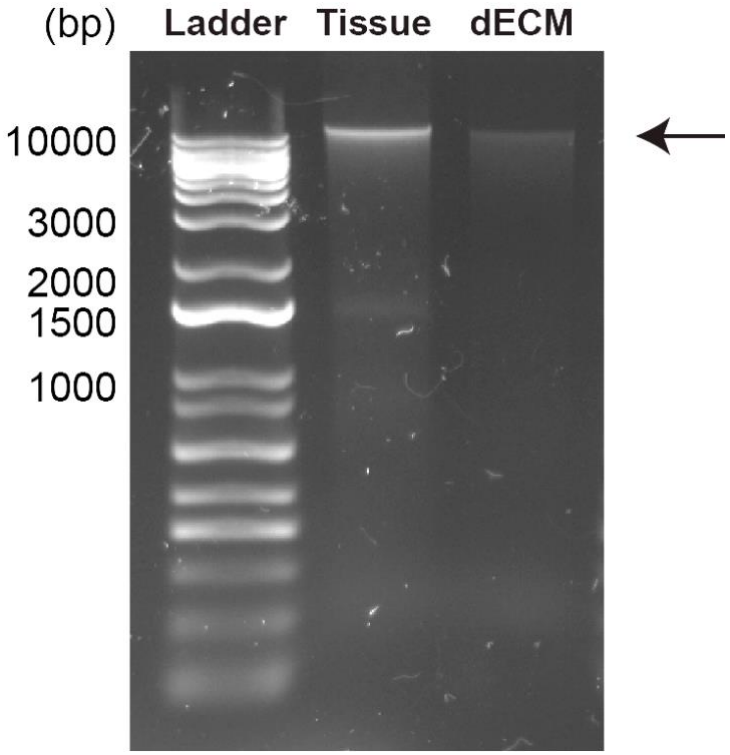


**Supplemental Figure 1. Decreased DNA content after 1% SDS decellularization.**

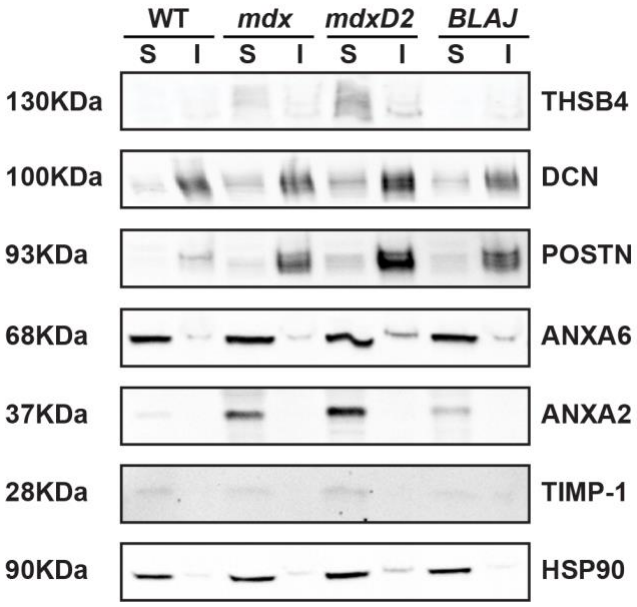


**Supplemental Figure 2. Immunoblot of soluble (S) and insoluble (I) muscle lysate fractions reveals enrichment of matrix associated proteins in dystrophic muscle.**